Crystal Structure of a Proteolytic Fragment of the Sensor Histidine Kinase NarQ

Ivan Gushchin, Igor Melnikov, Vitaly Polovinkin, Andrii Ishchenko, Valentin Gordeliy

crystals

MDPI

Article

Crystal Structure of a Proteolytic Fragment of the Sensor Histidine Kinase NarQ

Ivan Gushchin [1,*], Igor Melnikov [2,3], Vitaly Polovinkin [1,2,4,†], Andrii Ishchenko [2,‡] and Valentin Gordeliy [1,2,4,5,*]

1 Research Center for Molecular Mechanisms of Aging and Age-Related Diseases, Moscow Institute of Physics and Technology, 141700 Dolgoprudny, Russia
2 Institute of Biological Information Processing (IBI-7: Structural Biochemistry), Forschungszentrum Jülich, 52428 Jülich, Germany
3 European Synchrotron Radiation Facility, 38000 Grenoble, France
4 Institut de Biologie Structurale J.-P. Ebel, Université Grenoble Alpes-CEA-CNRS, 38000 Grenoble, France
5 JuStruct: Jülich Center for Structural Biology, Forschungszentrum Jülich, 52428 Jülich, Germany
* Correspondence: ivan.gushchin@phystech.edu (I.G.); valentin.gordeliy@ibs.fr (V.G.)
† Present address: ELI Beamlines, Institute of Physics, Czech Academy of Sciences, 18221 Prague, Czech Republic.
‡ Present address: Merck Research Laboratories, Merck and Co Inc., 770 Sumneytown Pike, West Point, PA 19486, USA.

Received: 3 February 2020; Accepted: 24 February 2020; Published: 27 February 2020

Abstract: Two-component signaling systems (TCSs) are a large and important class of sensory systems in bacteria, archaea, and some eukaryotes, yet their mechanism of action is still not fully understood from the structural point of view. Many TCS receptors are elongated flexible proteins with transmembrane (TM) regions, and are difficult to work with. Consequently, truncated fragments of the receptors are often used in structural studies. However, it is not fully clear whether the structures of the fragments correspond well to their native structures in the context of full-length proteins. Recently, we crystallized a fragment of *Escherichia coli* nitrate/nitrite sensor histidine kinase, NarQ, encompassing the sensor, TM, and HAMP domains. Here we report that a smaller proteolytic fragment consisting of the sensor and TM domains can also be crystallized using the in meso approach. The structure of the fragment is similar to the previously determined one, with minor differences in the vicinity of the truncation site. The results show that the crystallization of such sensor–TM fragments can be accomplished and can provide information on the packing of transmembrane helices, albeit limited, and that the proteolysis may or may not be a problem during crystallization.

Keywords: two-component systems; histidine kinase; transmembrane signaling; in meso crystallization; proteolysis

1. Introduction

Two-component signaling systems (TCSs) are a large and important class of sensory systems in bacteria, archaea, and some eukaryotes [1–4]. As their name implies, they generally consist of two parts: (i) a sensory protein or a complex of proteins, often embedded in the membrane, and (ii) a response regulator (RR) protein, which is phosphorylated or dephosphorylated depending on the nature of the signal. Phosphorylation is achieved by a histidine kinase (HK), which phosphorylates its own histidine amino acid, and then transfers the phosphate to the RR protein. The most common Class I HKs act independently, whereas Class II HKs act as a part of large arrays formed by chemoreceptors and accessory proteins. Class I HKs and chemoreceptors often employ the same sensory domains and, in the case of transmembrane (TM) sensors, the cytoplasmic HAMP domain as a signal transduction

module [5]. Overall, HKs have modular architecture; some minimalistic sensors consist of only three domains: sensor, dimerization/histidine phosphotransfer (DHp), and catalytic (CA), whereas more elaborate receptors have more domains, with TM, HAMP, PAS, and GAF domains interspersed between the sensor and DHp/CA domains [6–9]. Sensor proteins are inherently dynamic and can adopt multiple conformations; the presence of multiple domains and the transmembrane helices further complicates the structural studies. Consequently, no atomistic high-resolution structure of a full-length transmembrane TCS sensor protein has yet been determined experimentally, although several models were built using a combination of crystallography, electron microscopy, electron tomography, and molecular modeling [10–12]. In the absence of reliable models of full-length sensors in different signaling states, our understanding of the mechanisms of signal transduction in TCSs—especially across membranes—remains limited [5,8,9].

One of the popular approaches in structural studies of TCS proteins is the generation of truncated fragments encompassing one or more domains. Many structures of sensor domains of both chemoreceptors and histidine kinases in different signaling states have been determined, as well as those of intracellular modules such as HAMP, PAS, GAF, DHp, and CA [5–9]. Consequently, signal generation in the sensor domain and regulation of the catalytic domain are relatively well-understood. On the contrary, little direct structural information is available for the transmembrane fragments [5]. Experimentally determined atomic resolution structures obtained in the native state are available for only two proteins: *Escherichia coli* nitrate/nitrite sensor histidine kinase NarQ [13] and *Natronomonas pharaonis* sensory rhodopsin transducer HtrII [14,15]. Although the mechanism of the transmembrane signal transduction is most likely the piston-like motions of the TM helices [5], it is not clear whether it is general and how it is accomplished in the proteins from different subfamilies.

Recently, we crystallized a fragment of *E. coli* nitrate/nitrite sensor histidine kinase, NarQ, encompassing the sensor, TM, and HAMP domains and lacking the S-helix, GAF-like, DHp, and CA domains [13]. The protein was crystallized in three different forms—symmetric apo, symmetric holo, and asymmetric holo—which provided important structural data on TM signaling. Here we report that a smaller proteolytic fragment consisting of the sensor and TM domains could also be crystallized using the in meso approach and discuss the implications of this observation.

2. Materials and Methods

2.1. Cloning, Protein Expression, and Purification

Cloning, protein expression, and purification were performed exactly as described previously [13]. In short, the protein was expressed in *E. coli* using an auto-inducing medium [16] and purified using metal affinity (Ni-NTA) and size-exclusion chromatography. Protein-containing fractions were pooled and concentrated to 30 mg/mL for crystallization.

2.2. Mass Spectrometry

The matrix used for mass spectrometry contained 10 mg/mL sinapinic acid in a 50/50 *v*/*v* mixture of water and acetonitrile with 0.1% trifluoracetic acid. The sample was diluted 1:2 in the matrix and was deposited directly on the target. The sample was analyzed using a MALDI-TOF mass spectrometer (Autoflex, Bruker Daltonics, Bremen, Germany) operated in linear positive mode.

2.3. Crystallization

The crystals were grown using the in meso approach [17–19], similarly to our previous work [13]. The solubilized protein in the crystallization buffer was added to the monooleoyl-formed lipidic phase (Nu-Chek Prep, Elysian, MN, USA). Crystallization trials were set up using the NT8 robotic system (LCP version, Formulatrix, Bedford, MA, USA). The crystals were grown at 22 °C and reached the final size of ~100 µm within 3 months. The crystals were obtained using the precipitant solution consisting of 1 M KH_2PO_4/Na_2HPO_4 pH 5.2 and 5 mM $NaNO_3$. Before harvesting, the crystals were incubated

for 5 min in the respective precipitant solutions supplemented with 20% glycerol. All crystals were harvested using micromounts (MicroLoops HT, MiTeGen, Ithaca, NY, USA), then flash-cooled and stored in liquid nitrogen.

2.4. Acquisition and Treatment of Diffraction Data

The diffraction data were collected at 100 K at the European Synchrotron Radiation Facility (ESRF) beamline ID23-1 [20] equipped with a PILATUS 6M-F detector (Dectris, Baden-Daettwil, Switzerland). The data collection statistics are reported in Table 1. In all cases, the diffraction was anisotropic as determined by decay of the $CC_{1/2}$ values in 20° cones along the reciprocal cell directions [21]. Diffraction images were processed using XDS (version from 15 October 2015) [22]. XSCALE (version from 15 October 2015) [22] was used to merge different datasets and to scale the data for the phasing steps. POINTLESS (version 1.9.16) [21] and AIMLESS (version 0.3.11) [21] were used to merge, scale, assess the quality, convert intensities to structure factor amplitudes, and generate Free-R labels.

2.5. Structure Determination and Refinement

The structure was solved using molecular replacement with MOLREP (version 11.2.08) [23] and the sensor and transmembrane domains from the structure of the sensor–TM–HAMP fragment (Protein Data Bank Identifier 5IJI) [13] as a search model. The model was refined manually using Coot (version 0.7.2) [24] and REFMAC5 (version 5.8.0073) [25]. The refinement statistics are summarized in Table 1.

3. Results and Discussion

3.1. Expression and Proteolysis of a NarQ Fragment

Similarly to our previous work [13], we overexpressed the fragment of *E. coli* NarQ encompassing the sensor, TM, and HAMP domains (residues 1-230), and a 6xHis tag at the C-terminus, in its native host, *E. coli*. Following expression, the protein was solubilized and purified using immobilized metal affinity chromatography and size exclusion chromatography. Following purification, the protein migrated as two bands in SDS-PAGE gels: a major band corresponding to the expected molecular weight (MW), and a minor band at a lower MW (Figure S1). The major band could be stained using anti-His tag antibodies, whereas the minor band could not. Matrix-Assisted Laser Desorption/Ionization-Time Of Flight (MALDI-TOF) mass spectrometry revealed that the sample contained two species, the major one with MW of 26,751.5 Da, close to the expected MW of 26,780 Da, and the minor one with MW of 20,507 Da (Figure S2). Consequently, we assumed that the minor species corresponded to a proteolytic fragment of NarQ missing the HAMP domain and C-terminal His tag (residues 1-181 or 1-182, expected MW 20,407 or 20,535 Da, correspondingly) that was copurified in heterodimers with the intact His-tagged construct. The sample was used for in meso crystallization without further purification.

3.2. Crystallization of a Proteolytic NarQ Fragment

While trying to crystallize NarQ in the apo form, we attempted an extensive search for crystallization conditions. One of the identified conditions resulted in crystals that diffracted to the resolution of ~2 Å. Detailed analysis revealed that the crystals belong to the space group I4, and that their diffraction is anisotropic: cross-correlation CC1/2 reached 0.8 at 2.3 Å along the reciprocal axes a* and b*, and at 2.6 Å along axis c*. The data collection statistics are summarized in Table 1. The structure could be solved using molecular replacement with the structure of the sensor and TM domains from the previously determined structure of the sensor–TM–HAMP fragment of NarQ (PDB ID 5IJI [13]) as a search model, and revealed the positions of residues 13 to 170 comprising the sensor and TM domains. The NarQ fragments form membranelike layers in the crystals, as observed in type I crystals of other proteins grown in meso [18,19]. However, unlike in the previously obtained NarQ crystals, where neighboring proteins packed head-to-tail, in space group I4 the proteins packed head-to-head and in the same orientation (Figure 1a). While some residual densities were observed in the interlayer

space, no polypeptide chains could be traced there, and thus the nature of the contacts between the layers was not clear. Anisotropy of diffraction and faster decay of the diffraction quality along the reciprocal axis c* likely reflected the worse ordering in the direction normal to the layers.

Table 1. Crystallographic data collection and refinement statistics. R.m.s.: root mean square

Data Collection	
Space group	I4
Cell dimensions	-
a, *b*, *c* (Å)	51.28, 51.28, 182.99
α, β, γ (°)	90, 90, 90
Wavelength (Å)	0.9724
Resolution (Å)	49.38–2.30 (2.38–2.30)
R_{merge} (%)	5.8 (47.1)
R_{pim} (%)	4.5 (36.2)
$<I/\sigma I>$	13.2 (2.6)
CC1/2 (%)	99.9 (77.2)
Completeness (%)	97.8 (99.8)
Multiplicity	4.3 (4.4)
Unique reflections	10,245 (1015)
Refinement	
Resolution (Å)	49.38–2.30
No. reflections	9733
R_{work}/R_{free} (%)	24.9/28.5
No. atoms	-
Protein	1246
Water	81
Average *B* factors (Å^2)	-
Protein	71
Protein residues 37–145	50
Water	53
R.m.s. deviations	-
Protein bond lengths (Å)	0.004
Protein bond angles (°)	0.68
Ramachandran analysis	-
Favored (%)	98.7
Outliers (%)	0

3.3. Absence of the HAMP Domain in the Crystallized Fragment

No residual electron densities that could be ascribed to the HAMP domain were observed in the present data. Moreover, while there was enough space for the remaining TM helix residues (7–12 and 171–175) between the adjacent layers, there was not enough space for a folded nor an unfolded HAMP domain (Figure 1a). The unit cell size in the direction normal to the membrane was ~183 Å (~91.5 Å per layer), as opposed to 118–120 Å per layer in the previously obtained crystals of the sensor–TM–HAMP fragment (space groups $I2_12_12_1$, F222, and P2 [13]). Given that the protein sample that was used for crystallization contained a proteolyzed fraction, we concluded that the crystals likely corresponded to the proteolytic fragments. This was surprising, because homodimers of the proteolytic fragments could not be purified using metal affinity chromatography due to the lack of His tags, and thus could not be present in the original sample used for crystallization. Therefore, either the exchange of the protomers within the dimers could occur in the lipidic cubic phase during crystallization, or proteolysis was also happening after the setup of crystallization probes. Neither possibility can be excluded, as the I4 crystals appeared much slower, in ~3 months, compared to the $I2_12_12_1$, F222, and P2 crystals of sensor–TM–HAMP fragments that appeared in 1–2 weeks in similar conditions [13]. Another peculiarity was that the protein was proteolyzed despite being native to the expression host, *E. coli*, and no functional role of such proteolysis can be imagined at the moment.

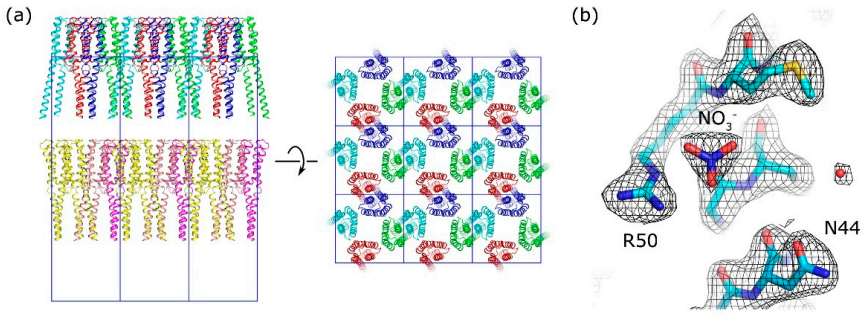

Figure 1. (**a**) Packing of the proteolytic fragment of NarQ in crystals in the space group I4. Symmetry-related molecules are colored differently. The proteins pack in parallel in layers. The remaining space between the protein layers was not sufficient to accommodate the missing HAMP domains. (**b**) An example of the $2F_o$-F_c electron density contoured at the 1.5 × r.m.s.

3.4. Structure of the Proteolytic NarQ Fragment

The determined structure reveals the positions of residues 13 to 170 and comprises the sensor and TM domains. The sensor domain is in the ligand-bound conformation with the nitrate ion bound in its pocket (Figure 1b). Overall, the structure is similar to the symmetrical holo structure determined previously (Figure 2a, position of the membrane boundaries is calculated using the PPM server [26]), with root-mean-square deviation (RMSD) of C_α positions of 1.0 Å and RMSD of the sensor domain C_α positions (residues 37–145) of 0.24 Å.

Whereas sensor-proximal ends of the TM helices are well-ordered and positioned similarly to those in the bigger fragment, the ends distant from the sensor domain are progressively disordered, having weaker electron densities and elevated B-factors. A small deviation from the symmetrical holo structure is observed at the cytoplasmic side, which could be best described as a diagonal scissoring-like displacement for ~1.5 Å (Figure 2b,c). This is likely a consequence of the lack of the HAMP domain and highlights the fact that scissoring-like motion is permitted in NarQ [5,13].

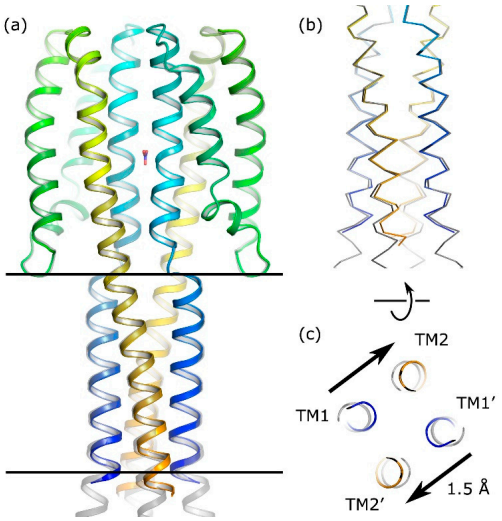

Figure 2. Differences in the transmembrane (TM) domain structures of the sensor–TM (rainbow coloring) and sensor–TM–HAMP (grey) constructs. (**a**) Overall comparison. Black lines show the approximate position of the membrane boundaries calculated using the PPM server [26]. (**b**) Comparison of the transmembrane regions. (**c**) Displacement of the cytoplasmic ends of the TM helices in the sensor–TM structure.

Recently, Pollard and Sourjik found that similar sensor–TM constructs of the *E. coli* chemoreceptor Tar (but not Tap) are able to cluster due to the interactions mediated by the TM helices [27]. We did not observe any interactions between the TM domains belonging to different NarQ dimers (Figure 1a),

however this likely reflects the fact that sensor histidine kinases do not require clustering for function, as opposed to bacterial chemoreceptors.

3.5. Impact of Truncation on the Structure

Several structures of bacterial nitrate sensors employing similar fold are currently available and allow us to estimate the effects of truncation. First, Cheung and Hendrickson determined the structure of the isolated sensor domain of the *E. coli* sensor histidine kinase NarX, closely related to NarQ, both in the ligand-free and the ligand-bound forms [28]. Second, Boudes et al. determined the structure of the full-length soluble transcription antiterminator protein NasR, which revealed that its NIT domain is structurally and functionally similar to the dimeric sensor domain of NarX [29]. Later, we determined the structure of a transmembrane fragment of NarQ [13]. Finally, Martín-Mora et al. determined the structure of the sensor domain PilJ of the *Pseudomonas aeruginosa* chemoreceptor McpN, which turned out to be similar to that of the previously characterized nitrate-binding proteins [30].

In McpN, NarX, and NarQ, the nitrate-binding domain is found in similar structural contexts (proximal to a bundle of 4 TM helices), whereas in NasR the context is different (the protein is soluble). Consequently, we compared only the homodimeric nitrate-bound structures of McpN, NarX, and NarQ. In all of these structures, the residues in the ligand-binding region are ordered the best, whereas the residues closer to the truncation site are progressively disordered (Figure 3). Positions of the sensor proximal parts of the helices TM2 in the NarX structure mirror those in the NarQ structures, and positions of the TM helices in the structure of the sensor–TM fragment mirror those in the structure of the sensor–TM–HAMP fragment. Still, the termini at the truncation sites lack some of the native interactions; they are less ordered and could be affected by crystal contacts. Consequently, the information on their conformations should be used with care.

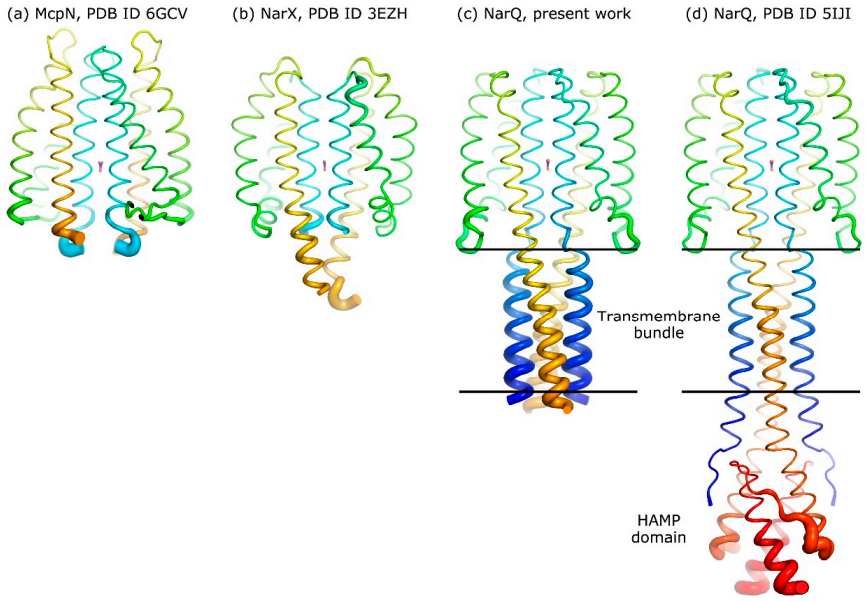

Figure 3. Disorder in the available crystallographic structures of fragments of nitrate-binding two-component signaling system (TCS) proteins. Thickness of the protein backbone tube is proportional to the B-factor. Rainbow coloring highlights the progression of the polypeptide chain from the N terminus (blue) towards the C terminus (red). (**a**) Sensor domain of McpN, PDB ID 6GCV [30]. B-factor range is 11–98 Å^2, average is 23 Å^2. (**b**) Sensor domain of NarX, PDB ID 3EZH [28]. B-factor range is 13–86 Å^2, average is 30 Å^2. (**c**) Sensor and TM domains of NarQ, present work. B-factor range is 20–192 Å^2, average is 71 Å^2 (20–122 Å^2 and 50 Å^2 for the sensor domain, correspondingly). (**d**) Sensor, TM, and HAMP domains of NarQ, PDB ID 5IJI [13]. B-factor range is 15–99 Å^2, average is 34 Å^2. Whereas the residues in the ligand-binding region are always well-ordered, the residues closer to the truncation site are progressively disordered.

3.6. Implications for Crystallization of TCS Sensors

Compared to the crystallization of soluble proteins, the crystallization of membrane proteins is hampered by the fact that the TM region of the protein must be embedded in the membrane, membrane mimic, or a detergent during purification and crystallization. For efficient crystallization, the protein molecules should form a three-dimensional network of contacts. Larger membrane proteins can be crystallized while being solubilized in detergent, similarly to soluble proteins. However, for smaller proteins, detergent micelles surrounding them shield the proteins from each other and preclude the formation of stable contacts. As a viable alternative, the in meso approach has been developed, reliant on the three-dimensional membranous cubic phases of special lipids that provide the medium for the proteins to diffuse and crystallize [17–19,31]. The approach has its own limitations, as the protein should fit into the cubic phase and should not be too big.

Full-length transmembrane TCS sensors reach hundreds of angstroms in length, and probably are too flexible for crystallization. Choosing the site of truncation to generate a crystallizable construct is not always easy and straightforward. The two major considerations are (i) that the fragment should not be too flexible, and (ii) that the structure of the fragment should generate the required information. If only the information on the ligand binding mode is being sought, then the crystallization of a solitary sensor domain is sufficient. However, for studies of the signal transduction, not only the structures of the individual domains in the signaling and inactive states of the protein should be determined, but also the structures of the linkers between them. The structure of the sensor–TM linker was the same in the proteolytic fragment studied here and in the previously determined structure of the sensor–TM–HAMP fragment. The structure of the TM–HAMP linker was the same in the previously determined structure and the structure of the TM–HAMP fragment of the protein Af1503 [32]. Yet, for crystallization, a fragment with the intact domains at both sides of the membrane is preferable, so that stable contacts can be formed between the proteins from different membranous layers: the sensor–TM–HAMP fragment of NarQ crystallized better and the crystals diffracted to a higher resolution [13] compared to the sensor–TM fragment presented here.

4. Conclusions

Our results clearly show that minimalistic TM fragments encompassing sensor and TM domains could be crystallized and could provide some information on the packing of the receptor transmembrane helices. The inclusion of a cytoplasmic domain would be preferable to fix the cytoplasmic ends of the TM helices in the correct arrangement. Partial proteolysis and the resulting impurity in the sample can have consequences for the crystallization of the original construct, as evidenced by the previously obtained structures [13]. The crystals of a proteolytic fragment could also be obtained from the same sample, but the information gained from the structure of this fragment would be inferior compared to the information gained from structures of bigger fragments.

Supplementary Materials: Supplementary Figure S1 (SDS-PAGE of the NarQ sample used for crystallization) and Figure S2 (MALDI-TOF MS spectrum of the NarQ sample used for crystallization) are available online at http://www.mdpi.com/2073-4352/10/3/149/s1.

Author Contributions: Conceptualization, I.G. and V.G.; investigation, I.G., I.M., V.P., and A.I.; resources, I.G. and V.G.; writing—original draft preparation, I.G.; writing—review and editing, I.G. and V.G.; supervision, I.G. and V.G.; project administration, I.G. and V.G.; funding acquisition, I.G. and V.G. All authors have read and agreed to the published version of the manuscript.

Funding: This research was funded by the Russian Science Foundation, grant number 18-74-10053. We acknowledge the platforms of the Grenoble Instruct Center (ISBG; UMS 3518 CNRS-CEA-UJF-EMBL) supported by the French Infrastructure for Integrated Structural Biology Initiative FRISBI (ANR-10-INSB-05-02) and GRAL (ANR-10-LABX-49-01) within the Grenoble Partnership for Structural Biology (PSB). The study (I.M.) was supported by ESRF PhD and in-house research programs.

Acknowledgments: Atomic coordinates and structure factors for the reported crystal structure have been deposited with the Protein Data Bank under the accession code 6XYN. The diffraction experiments were performed on beamline ID23-1 at the European Synchrotron Radiation Facility (ESRF), Grenoble, France. We are grateful to Alexander Popov for providing assistance in using this beamline.

Conflicts of Interest: The authors declare no conflict of interest. The funders had no role in the design of the study; in the collection, analyses, or interpretation of data; in the writing of the manuscript; or in the decision to publish the results.

References

1. Wuichet, K.; Cantwell, B.J.; Zhulin, I.B. Evolution and phyletic distribution of two-component signal transduction systems. *Curr. Opin. Microbiol.* **2010**, *13*, 219–225. [CrossRef] [PubMed]
2. Capra, E.J.; Laub, M.T. Evolution of two-component signal transduction systems. *Annu. Rev. Microbiol.* **2012**, *66*, 325–347. [CrossRef] [PubMed]
3. Schaller, G.E.; Shiu, S.-H.; Armitage, J.P. Two-component systems and their co-option for eukaryotic signal transduction. *Curr. Biol.* **2011**, *21*, R320–R330. [CrossRef] [PubMed]
4. Papon, N.; Stock, A.M. Two-component systems. *Curr. Biol.* **2019**, *29*, R724–R725. [CrossRef] [PubMed]
5. Gushchin, I.; Gordeliy, V. Transmembrane signal transduction in two-component systems: Piston, scissoring, or helical rotation? *BioEssays* **2018**, *40*, 1700197. [CrossRef] [PubMed]
6. Bhate, M.P.; Molnar, K.S.; Goulian, M.; DeGrado, W.F. Signal transduction in histidine kinases: Insights from new structures. *Structure* **2015**, *23*, 981–994. [CrossRef] [PubMed]
7. Zschiedrich, C.P.; Keidel, V.; Szurmant, H. Molecular mechanisms of two-component signal transduction. *J. Mol. Biol.* **2016**, *428*, 3752–3775. [CrossRef]
8. Jacob-Dubuisson, F.; Mechaly, A.; Betton, J.-M.; Antoine, R. Structural insights into the signalling mechanisms of two-component systems. *Nat. Rev. Microbiol.* **2018**, *16*, 585–593. [CrossRef]
9. Buschiazzo, A.; Trajtenberg, F. Two-component sensing and regulation: How do histidine kinases talk with response regulators at the molecular level? *Annu. Rev. Microbiol.* **2019**, *73*, 507–528. [CrossRef]
10. Cassidy, C.K.; Himes, B.A.; Sun, D.; Ma, J.; Zhao, G.; Parkinson, J.S.; Stansfeld, P.J.; Luthey-Schulten, Z.; Zhang, P. Structure and dynamics of the E. coli chemotaxis core signaling complex by cryo-electron tomography and molecular simulations. *Commun. Biol.* **2020**, *3*, 1–10. [CrossRef]
11. Orekhov, P.; Bothe, A.; Steinhoff, H.-J.; Shaitan, K.V.; Raunser, S.; Fotiadis, D.; Schlesinger, R.; Klare, J.P.; Engelhard, M. Sensory rhodopsin I and sensory rhodopsin II form trimers of dimers in complex with their cognate transducers. *Photochem. Photobiol.* **2017**, *93*, 796–804. [CrossRef] [PubMed]
12. Akkaladevi, N.; Bunyak, F.; Stalla, D.; White, T.A.; Hazelbauer, G.L. Flexible hinges in bacterial chemoreceptors. *J. Bacteriol.* **2018**, *200*, e00593-17. [CrossRef] [PubMed]
13. Gushchin, I.; Melnikov, I.; Polovinkin, V.; Ishchenko, A.; Yuzhakova, A.; Buslaev, P.; Bourenkov, G.; Grudinin, S.; Round, E.; Balandin, T.; et al. Mechanism of transmembrane signaling by sensor histidine kinases. *Science* **2017**, *356*, eaah6345. [CrossRef] [PubMed]
14. Gordeliy, V.I.; Labahn, J.; Moukhametzianov, R.; Efremov, R.; Granzin, J.; Schlesinger, R.; Büldt, G.; Savopol, T.; Scheidig, A.J.; Klare, J.P.; et al. Molecular basis of transmembrane signalling by sensory rhodopsin II—Transducer complex. *Nature* **2002**, *419*, 484–487. [CrossRef]
15. Ishchenko, A.; Round, E.; Borshchevskiy, V.; Grudinin, S.; Gushchin, I.; Klare, J.P.; Remeeva, A.; Polovinkin, V.; Utrobin, P.; Balandin, T.; et al. New insights on signal propagation by sensory rhodopsin II/transducer complex. *Sci. Rep.* **2017**, *7*, 41811. [CrossRef]
16. Studier, F.W. Protein production by auto-induction in high-density shaking cultures. *Protein Expr. Purif.* **2005**, *41*, 207–234. [CrossRef]
17. Gordeliy, V.I.; Schlesinger, R.; Efremov, R.; Büldt, G.; Heberle, J. Crystallization in lipidic cubic phases. In *Membrane Protein Protocols: Expression, Purification, and Characterization*; Selinsky, B., Ed.; Humana Press: Totowa, NJ, USA, 2003.
18. Caffrey, M. A comprehensive review of the lipid cubic phase or in meso method for crystallizing membrane and soluble proteins and complexes. *Acta Crystallogr. Sect. F Struct. Biol. Commun.* **2015**, *71*, 3–18. [CrossRef]
19. Ishchenko, A.; Abola, E.E.; Cherezov, V. Crystallization of membrane proteins: An overview. In *Protein Crystallography: Methods and Protocols*; Wlodawer, A., Dauter, Z., Jaskolski, M., Eds.; Humana Press: New York, NY, USA, 2017; pp. 117–141. ISBN 978-1-4939-7000-1.
20. Nurizzo, D.; Mairs, T.; Guijarro, M.; Rey, V.; Meyer, J.; Fajardo, P.; Chavanne, J.; Biasci, J.-C.; McSweeney, S.; Mitchell, E. The ID23-1 structural biology beamline at the ESRF. *J. Synchrotron Radiat.* **2006**, *13*, 227–238. [CrossRef]

21. Evans, P. Scaling and assessment of data quality. *Acta Crystallogr. D Biol. Crystallogr.* **2005**, *62*, 72–82. [CrossRef]
22. Kabsch, W. XDS. *Acta Crystallogr. D Biol. Crystallogr.* **2010**, *66*, 125–132. [CrossRef]
23. Vagin, A.; Teplyakov, A. Molecular replacement with MOLREP. *Acta Crystallogr. D Biol. Crystallogr.* **2009**, *66*, 22–25. [CrossRef] [PubMed]
24. Emsley, P.; Cowtan, K. Coot: Model-building tools for molecular graphics. *Acta Crystallogr. D Biol. Crystallogr.* **2004**, *60*, 2126–2132. [CrossRef] [PubMed]
25. Murshudov, G.N.; Skubák, P.; Lebedev, A.A.; Pannu, N.S.; Steiner, R.A.; Nicholls, R.A.; Winn, M.D.; Long, F.; Vagin, A.A. REFMAC5 for the refinement of macromolecular crystal structures. *Acta Crystallogr. D Biol. Crystallogr.* **2011**, *67*, 355–367. [CrossRef] [PubMed]
26. Lomize, M.A.; Pogozheva, I.D.; Joo, H.; Mosberg, H.I.; Lomize, A.L. OPM database and PPM web server: Resources for positioning of proteins in membranes. *Nucleic Acids Res.* **2012**, *40*, D370–D376. [CrossRef]
27. Pollard, A.M.; Sourjik, V. Transmembrane region of bacterial chemoreceptor is capable of promoting protein clustering. *J. Biol. Chem.* **2018**, *293*, 2149–2158. [CrossRef]
28. Cheung, J.; Hendrickson, W.A. Structural analysis of ligand stimulation of the histidine kinase NarX. *Structure* **2009**, *17*, 190–201. [CrossRef]
29. Boudes, M.; Lazar, N.; Graille, M.; Durand, D.; Gaidenko, T.A.; Stewart, V.; van Tilbeurgh, H. The structure of the NasR transcription antiterminator reveals a one-component system with a NIT nitrate receptor coupled to an ANTAR RNA-binding effector. *Mol. Microbiol.* **2012**, *85*, 431–444. [CrossRef]
30. Martín-Mora, D.; Ortega, Á.; Matilla, M.A.; Martínez-Rodríguez, S.; Gavira, J.A.; Krell, T. The molecular mechanism of nitrate chemotaxis via direct ligand binding to the PilJ domain of McpN. *mBio* **2019**, *10*, e02334-18. [CrossRef]
31. Landau, E.M.; Rosenbusch, J.P. Lipidic cubic phases: A novel concept for the crystallization of membrane proteins. *Proc. Natl. Acad. Sci. USA* **1996**, *93*, 14532–14535. [CrossRef]
32. Hartmann, M.D.; Dunin-Horkawicz, S.; Hulko, M.; Martin, J.; Coles, M.; Lupas, A.N. A soluble mutant of the transmembrane receptor Af1503 features strong changes in coiled-coil periodicity. *J. Struct. Biol.* **2014**, *186*, 357–366. [CrossRef]